Chalcogenide Letters Vol. 13, No. 11, November 2016, p. 521 - 528

PREPARATION AND PROPERTIES OF $ZnSe_xTe_{1-x}$ ALLOY THIN FILMS BY SOLID STATE REACTIONS

Y. YANG, Y. HU, C. LIU*, W. LI, J. ZHANG, L. WU, J. YANG
College of Materials Science and Engineering, Sichuan University, Chengdu 610064, China

Ternary $ZnSe_xTe_{1-x}$ alloy thin films were synthesized by solid state reactions and then the films were annealed at different temperatures in N_2 ambient. The structural, morphological, and optical properties of ZnSe/ZnTe multilayers were investigated by X-ray diffraction, scanning electron microscopy, and optical transmittance spectra. The results reveal that the strong inter-diffusion occurred between the ZnSe and ZnTe layers at high annealing temperatures. The annealing could promote the evolution of ZnSe and ZnTe into $ZnSe_xTe_{1-x}$ leading to the crystalline $ZnSe_xTe_{1-x}$ alloy thin films at 550℃. The optical parameters, such as refractive index, dispersion energy, absorption coefficients and optical band gap, were determined alone from the transmission spectrum of $ZnSe_xTe_{1-x}$ thin films.

(Received October 4, 2016; Accepted November 25, 2016)

Keywords: ZnSeTe Thin Films; Solid State Reactions; Material Characterization; Intermediate Band Solar Cell

1. Introduction

High-efficiency and low-cost solar cells are required in order to economically compete with conventional energy sources such as fossil and petroleum fuels. In the framework of the third generation of photovoltaic devices, the intermediate band solar cell (IBSC) provides new insight into the conversion efficiencies and offers a potential way to increase the limiting efficiency of a single gap solar cell from 30% to >60%[1-3]. ZnTe, one of the attractive materials of a blue-green emitting devices, is also applicable for IBSC. Previous work [4] reported that ZnTe:O IBSCs utilized energies below the band-gap energy and increased conversion efficiency of solar cells compared to the conventional devices, which are focused on direct valence to conduction band optical transitions[5]. However, defects from the large lattice mismatch of the active region and GaAs substrate leads to the low overall conversion efficiency of IBSCs based on ZnTe:O. Therefore, as one of the candidate materials of IBSCs, lattice matching has to be considered and $ZnSe_xTe_{1-x}$ was chosen in this work as the promising materials.

The ternary $ZnSe_xTe_{1-x}$ alloys have attracted a reasonable interest due to their unusual feature in the structural and optical properties[6-12]. Ahrenkiel et al. [6] studied spectacular atomic ordering that a compositionally modulated $ZnSe_xTe_{1-x}$ superlattice was self-organized in the $ZnSe_{0.5}Te_{0.5}$ specimens. A series of spontaneous ordering results was also found in a different band bowing by Freytag and co-workers[7]. Some researchers [8-10] reported a very broad photoluminescence(PL) structure for $ZnSe_xTe_{1-x}$ at a high Te content, attributing to the recombination of the Te-bound exciton which could be generally explained by a configuration coordinate diagram. Walukiewicz et al [11] found that a nonlinear pressure dependence of the band gaps and large downward shifts of the conduction band edges as functions of composition in $ZnSe_xTe_{1-x}$ systems. The dependencies are explained by an interaction between localized A_1 symmetry states of Se atoms and the extended states of the ZnTe matrix. Nassour [12]reported *ab initio* calculations of the structural properties and lattice dynamics of $ZnSe_xTe_{1-x}$. The two modes were observed in the *ab initio* spectrum, which are attributed to the bimodal behavior ($TO^{\mathrm{Se}}_{\mathrm{ZnSe}}$ and $TO^{\mathrm{Te}}_{\mathrm{ZnSe}}$) of the shortest bond.

* Corresponding author: liucaicn@foxmail.com

Many techniques, such as molecular beam epitaxy [13-15], Bridgman method [11, 16], vacuum evaporation [6,17], have been used to prepare $ZnSe_xTe_{1-x}$ solid solutions. It has been found that there are discrepancies in the optoelectrical characteristics (e.g., the energy band gap [10]). It is not clear whether the discrepancies originated from the preparation methods. For example, ingots of complete solid solutions of $ZnSe_xTe_{1-x}$ were firstly synthesized, and then obtained ingots were used as a source material for the preparation of samples in thin film form by thermal evaporation technique [17]. Due to the differences in the saturated vapor pressures of the pure binary constituents, direct vacuum evaporation of $ZnSe_xTe_{1-x}$ alloy may be not appropriate. In this paper $ZnSe_xTe_{1-x}$ thin films were synthesized by solid state reactions using electron beam evaporation. Annealing was adopted to acquire polycrystalline films by different temperatures in N_2 ambient. Structural, morphological and optical properties of the alloy films were investigated in this work.

2. Experimental details

The multilayer ZnSe/ZnTe films with a stacking sequence ZnSe-ZnTe-ZnSe. . . were deposited independently and alternately by electron beam evaporation at room temperature using high purity ZnSe powder (99.999% purity, Alfa Aesar) and ZnTe powder (99.999% purity, Alfa Aesar). The deposition rates of ZnSe and ZnTe were monitored by two thickness monitors. The total thickness of the multilayer thin films was about 300 nm, which includes ten cycles of ZnSe and ZnTe. After deposition, the multilayer thin films were annealed at different temperatures in N_2 ambient. The temperatures reproducible to ±1 ℃ were obtained from repeated runs on the same sample.

The structural properties of the films were investigated by X-ray diffraction (XRD, DX-2600, Dandong, China) using Cu Ka radiation (λ=1.5405 Å).The film thickness was measured with a stylus surface profiler (Ambios Technology Inc., XP-2). The surface morphologies of samples were observed at a low accelerating voltage (i.e., 5 kV) by a field emission scanning electron microscope (SEM, S-4800, Hitachi, Japan). Optical transmission was measured in the 300~2000 nm range using a UV/Vis/Nir spectrometer (Lambda 950, Perkin Elemer, USA).

3. Results and discussion

3.1 Structural properties

Fig. 1 shows the XRD patterns of the ZnSe-ZnTe multilayers obtained by using CuKα (λ≈0.15405 nm) radiation. As shown in Fig. 1(a) no crystalline $ZnSe_xTe_{1-x}$ compound was generated after deposition, in which only two diffraction peaks have been observed with 2θ values at the positions of 25.27° and 27.22°, corresponding to ZnTe(111) (JCPDS#15-746)and ZnSe(111) (JCPDS#5-522) starting material phases. The oriented growth of ZnSe and ZnTe indicates the relatively low surface energy of (111) planes, which benefit the formation of crystalline $ZnTe_xSe_{1-x}$ ternary compound. In order to form $ZnSe_xTe_{1-x}$ ternary alloys, thermal post-deposition treatment was performed. The as-deposited thin films on the soda-lime glass substrates were annealed in the range from 400°C to 550°C in N_2 ambient, respectively. Figures 1(b)~(d) show that subsequent annealing plays a key role in the formation of crystalline $ZnSe_xTe_{1-x}$ compound. Diffraction patterns of the films annealed at 400℃ have similar feature with that of the as-deposited sample, although the intensity of both peaks become stronger (Figure 1(b)).The XRD pattern features of samples annealed at 500℃ and 550℃ become distinctive. For sample annealed at 500℃(Figure 1(c)), the positions of ZnTe and ZnSe diffraction peaks are to combine as one, which could be reckoned that thermal annealing accelerates the particles inter-diffusion and promotes renewed structure. While raising annealing temperature to 550℃(Figure 1(d)), the diffraction pattern shows a polycrystalline structure with the strongest diffraction peak of a 2θ value at 25.5°, which corresponds to $ZnSe_xTe_{1-x}$ (111) planes. And two weak peaks occur at this temperature, which

correspond to $ZnSe_xTe_{1-x}$ (200) and (220) planes. The (*hkl*) planes of $ZnSe_xTe_{1-x}$ thin films were accorded with the following relation:

$$\frac{sin^2\theta}{h^2+k^2+l^2} = \frac{\lambda}{4a^2} \tag{1}$$

where $\lambda^2/4a^2$ is constant for any given patterns, (hkl) are the Miller indices with permissible values of the cubic structure and θ is the Bragg angle. The chemical reaction that took place in the thin binary constituent layers can be described as:

$$(1-x)\ ZnTe + x\ ZnSe \rightarrow ZnSe_xTe_{1-x} \tag{2}$$

This behavior is similar to that observed in Cu/Te multi-layers [18]. For higher annealing temperature, quartz glass substrates were used to replace soda-lime glass substrates to investigate the structural properties of $ZnSe_xTe_{1-x}$ thin films (Figures 1(e)-(g)). Annealing at 450℃two peaks at 2θ≈ 25.27° and 27.22°corresponding to the ZnTe(111) and ZnSe(111) planes appeared, which is not dissimilar from the behavior observed there for the sample on the soda-lime glass substrates as shown in Fig.1(b). The single phase $ZnSe_xTe_{1-x}$ thin films with a preferred (111) orientation were obtained at 650℃ in Figure 1(f), where small maxima peaks become evidently invisible compared to the films annealed at 550℃ on soda-lime glass substrates. A stronger diffraction peak displayed for samples annealed at 700℃, which also shows a preferential orientation (Figure 1(g)). One can see that an effect of the annealing temperature on the structure of the thin films, annealing at a higher temperature, would readily promote the formation of single-phase $ZnSe_xTe_{1-x}$ with very strong (111) preferential orientation.

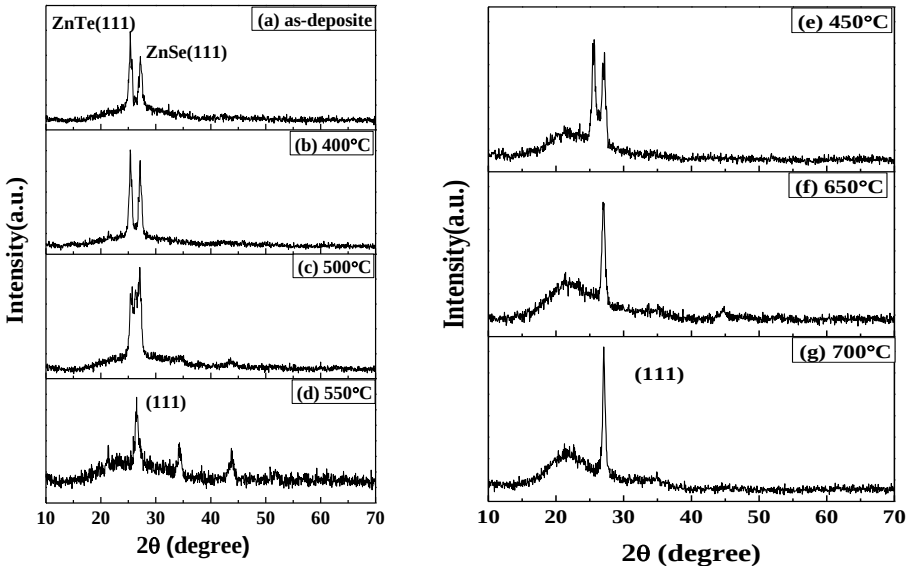

Fig. 1. XRD patterns of ZnSe/ZnTe multilayers on soda-lime glass (a~d) and quartz glass substrates (e-g) annealed at different temperatures for 15min in N_2 ambient.

The molecular fraction x can be estimated by the calculated unit cell lattice constant $a_{ZnSe_xTe_{1-x}}$ using Vegard's law:

$$x_{ZnSe_xTe_{1-x}} = \frac{a_{ZnSe_xTe_{1-x}} - a_{ZnTe}}{a_{ZnSe} - a_{ZnTe}} \times 100\% \tag{3}$$

where a_{ZnSe}, a_{ZnTe} are, respectively, the lattice constants of ZnSe, ZnTe. Therefore, from Eqs. (1) and (3), one can obtain the lattice constant of $ZnSe_xTe_{1-x}$ thin films a≈0.575 nm, and the molecular fraction x (≈0.86) of the thin films.

3.2 Morphologies

Scanning electron microscope was used to observe the morphologies of the thin films. Fig. 2 shows the SEM micrographs of ZnTe/ZnSe multilayer thin films in different annealing conditions. Figures 2(a)~2(d) display the surface morphology (magnification 100K×) and Fig.s 2(e)~2(h) show the corresponding cross-sectional images of ZnTe/ZnSe multilayer films(magnification 50.0K×). The as-deposited thin film shows a granular surface (Figure 2a) and a simple stacking multilayer microstructure from the cross-sectional SEM image(Figure 2e). In contrast, a thin compact surface with an average size of 200 nm has been observed for the films annealed at 300℃(Figure 2b), which has a mainly transgranular interface between ZnSe and ZnTe(Figure 2f) [19]. The transgranular fracture of intermediate layers is closely relevant to columnar grains, which can be attributed to the oriented (111) growth of ZnSe and ZnTe in combination with the analysis of XRD patterns. The average particle size becomes larger to 500 nm with a smooth morphology for the films upon increasing annealing temperature to 500℃(Figure 2c) and width of interlayer columnar grains becomes bigger (Figure 2g). Figure 2(d) shows the surface morphology of films annealed at 650℃ in channels linked together, which may be due to coalescence processes that the grains come close to each other and the larger ones merge the smaller ones motivated by the heat treatments [20]. Also, remarkable features are shown in Fig.2(h), in which the massive bulk grains are clearly visible. Obviously, the post-treatment process can promote the growth of the films, which is significant to reduce the grain boundary density. Combining with the XRD patterns of films annealed at 650℃(Figure 2b), we believe that high thermal temperature enhances the diffusion of activated atoms from ZnSe and ZnSe layers, thus nucleation of the intermediate alloy is then the rate-limiting step in forming the crystalline compound at a high temperature [21].

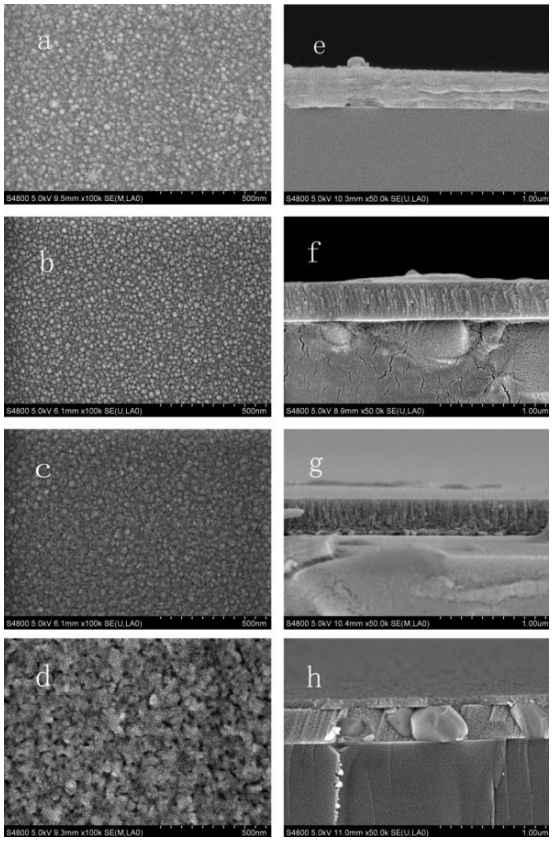

Fig. 2. SEM micrographs of surface morphology (a~d) and cross-sectional images (e~h) of ZnSe/ZnTe multilayer films on quartz glass substrates annealed at different temperatures: (a)(e) as-deposited , (b)(f) 300℃, (c)(g)500℃, (d)(h)650℃.

3.3 Optical properties

To investigate the optical properties of single phase polycrystalline $ZnSe_xTe_{1-x}$ films, the refractive index, n, thickness, d, absorption coefficient, α, and optical band gap, E_g were calculated from the transmission spectra of samples annealed at 650 ℃ using Swanepoel's method [22]. According to the method, the envelope of the transmission spectrum was acquired by numerical fitting of optical transmittance in maxima and minima interference fringes, respectively (Fig. 3) . In the spectral range of weak and medium absorption, the approximate value of the refractive index of the $ZnSe_xTe_{1-x}$ thin films, n, can be calculated by the expression,

$$n = \sqrt{E + \sqrt{E^2 - n_s^{\,2}}} \tag{4}$$

where $E = 2n_s \dfrac{T_M - T_m}{T_M \times T_m} + \dfrac{n_s^{\,2}+1}{2}$, T_M and T_m are the transmission maximum and the corresponding minimum at a certain wavelength λ from the envelope curve, and n_s (=1.533) is the refractive index of the glass.

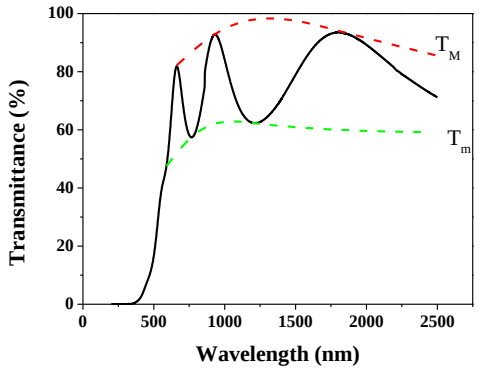

Fig. 3. Measured transmission spectrum of $ZnSe_xTe_{1-x}$ annealed at 650 ℃ and its envelopes T_M , T_m .

The order j of adjacent maxima (or minima) interference fringes conform to the following relation:

$$j\lambda_j = (j+1)\lambda_{j+1} \tag{5}$$

where the orders j of maxima (minima) interference fringes are integer (half-integer).
With the value of refractive index n and fringe orders j , the film thickness d can be figured by

$$2nd = j\lambda_j \tag{6}$$

The calculated thickness value of the $ZnSe_xTe_{1-x}$ thin film is about 368.48 nm and in return, the refractive index n in each maxima and minima interference fringe can be obtained according to Eq. (6).

The dispersion of the refractive index n are described according to the single-oscillator model deduces by Wemple and DiDomenico [23]:

$$n^2 - 1 = \frac{E_{osc} E_d}{{E_{osc}}^2 - (h\nu)^2} \tag{7}$$

where E_{osc} is the single-oscillator energy, E_d is the dispersion energy and $h\nu$ is the photon energy. Figure 4 shows the numerical fitting of the calculated refractive index n to a straight line, which is in accordance with Eq. (7). Furthermore, the values of E_{osc} (≈3.64 eV)and E_d (≈17.19 eV) can be obtained from the intercept, E_{osc} / E_d and the slope, $-1/E_{osc}E_d$.

The absorption coefficient, α, in the weak and medium absorption regions can be determined using the following relation,

$$\alpha = -\frac{1}{d} \ln \frac{Y - \sqrt{Y^2 - (n^2-1)^3 (n^2 - {n_s}^4)}}{(n-1)^3 (n - {n_s}^2)} \tag{8}$$

where n_s is the substrate refractive index(as above), d the thickness of the thin films, and n the refractive index of the films, and

$$Y = \frac{8n^2 n_s}{T_M} + (n^2 - 1)(n^2 - {n_s}^2) \tag{9}$$

In the spectral range of strong absorption, the Eq. (8) could be simplified as follows:

$$\alpha = -\frac{1}{d} \ln \left[\frac{(n+1)^3 (n + {n_s}^2)}{16 n^2 n_s} T \right] \tag{10}$$

where T is the transmittance of the films in the strong absorption region.

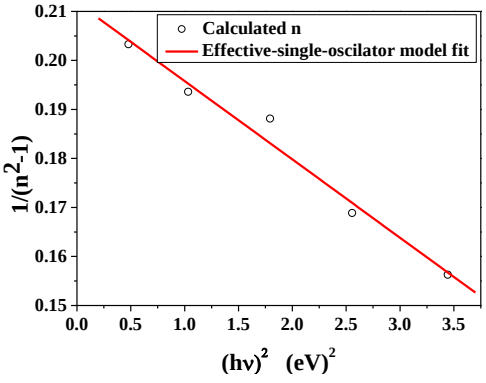

Fig. 4. Spectral dependences of refractive index n of radiation for $ZnSe_xTe_{1-x}$ thin films annealed at 650℃ with the effective single-oscillator mode.

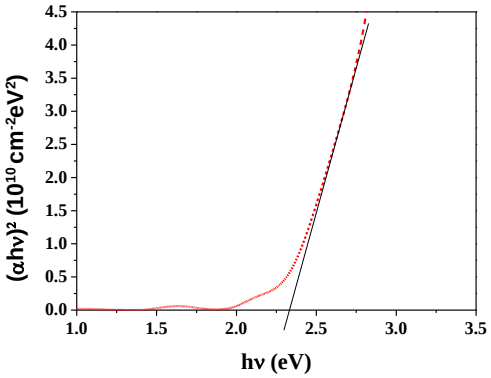

Fig.5. Dependence of $(\alpha h\nu)^2$ *on photon energy* $h\nu$ *to determine the optical band gap* E_g *for* $ZnSe_xTe_{1-x}$ *thin films annealed at 650℃.*

The absorption coefficient α with the energy of the photon hυ could be expressed by the following equation:

$$\alpha h\upsilon \propto (h\upsilon - Eg)^n \tag{11}$$

where α is the absorption coefficient, and the exponent n may take values, 1, 2, 3, 1/2, 3/2, depending on the electronic transitions in k- space. A linear fit is achieved for the $ZnSe_xTe_{1-x}$ thin films with n=1/2, indicating this material is a direct gap semiconductor. So $(\alpha h\upsilon)^2$ is plotted a function of hυ for $ZnSe_xTe_{1-x}$ thin films (Fig. 5). The optical band energy gap can be determined from the intercept of the extrapolation of the straight portion to the hυ axis. The approximate value of optical band gap E_g is 2.34 eV, which is a good agreement with the result that reported on another $ZnSe_xTe_{1-x}$ alloy systems in the epilayers by Brail et al. [13] and in single crystals by Su [10]. However, it ismuch smaller than that reported on ZnSeTe alloy systems in thin films by El-Nahass et al. [17]. The discrepancy in the band gap might be ascribed to the effect of strain and temperature on the thin films [7,10,13, 17]. Theoretical calculations [1] indicate that the optimum gap for photovoltaic energy conversion at 1 sun appears at 2.41 eV with the intermediate band located at 0.92 eV from the conduction band (or valence band) and exhibiting a potential efficiency of 46.77%. In this view, $ZnSe_xTe_{1-x}$ (x~0.86), with a band gap of 2.34 eV and a limiting efficiency of 46.7% approaches this optimum very well.

4. Conclusions

The $ZnSe_xTe_{1-x}$ thin films were deposited at room temperature by solid state reactions using electron beam evaporation with an alternative ZnSe/ZnTe multilayer structure. To promote the inter-diffusion of ZnSe and ZnTe, as-deposited thin films were annealed at high temperatures in N_2 ambient. The films annealed at 550℃ were polycrystalline in random crystallographic directions. The optical parameters were obtained alone from the transmission spectrum of the $ZnSe_xTe_{1-x}$ thin films. The thickness of the $ZnSe_xTe_{1-x}$ thin film is about 368.48 nm and the single-oscillator energy and the dispersion energy are about 3.64 and 17.19 eV, respectively. The value of optical band gap E_g (≈2.34 eV) for the thin films in a direct transitions type was determined by the analysis of absorption data. The difference in the band gap between the bulk and film might be due to the strain and temperature effects. The studies of dilute oxygen $ZnSe_xTe_{1-x}$ (x~0.86) thin films for IBSCs are under way.

Acknowledgements

This work was supported by the National High Technology Research and Development Program of China (Grant no.2015AA050610), and Science and Technology Program of Sichuan Province, China (Grant No. 2016GZX0272).

References

[1] A Marti, David Fuertes Marron, A. Luque, J Appl Phys **103**, 073706 (2008).
[2] A Luque, A Marti, N Lopez, E Antolin, E Canovas, L J Caballero, L Cuadra, J L Balenzategui, Appl Phys Lett **87**, 083505 (2005).
[3] S Yagi, S, Noguchi, Y Hijikata, S Kuboya, K Onabe, H Yaguchi, Jpn J Appl Phys **52,** 102302 (2013).
[4] Weiming Wang, Albert S. Lin, Jamie D. Phillips, Appl. Phys. Lett. **95**, 011103 (2009).
[5] Albert S. Lin, Weiming Wang, Jamie D. Phillips, J. Appl. Phys. **105**, 064512 (2009).
[6] S P Ahrenkiel, S H Xin, P M Reimer, J J Berry, H Luo, S Short, M Bode, M Al-Jassim, J R Buschert, J K Furdyna, Phys Rev B **43**, 4396 (1991).
[7] B Freytag, P Pavone, U Rossler, K Wolf, S Lankes, G Schotz, A Naumov, S Jilka, W Gebhardt, Solid State Commun **94**, 103 (1995).
[8] T Yao, M Kato, J J Davies, H Tanino, J Cryst Growth **86**, 552 (1988).
[9] C. S. Yang, D. Y. Hong, C. Y. Lin, W. C. Chou, C. S. Ro, J. Appl. Phys. **83,** 2555 (1998).
[10] Ching-hua Su, S Feth, Shen Zhu, S L Lehoczky, Lin Jun Wang, J Appl Phys **88,** 5148 (2000).
[11] W. Walukiewicz, W. Shan, K. M. Yu, and J.W. Ager III, E. E. Haller, I. Miotkowski, M. J. Seong, H. Alawadhi, A. K. Ramdas, Phys Rev Lett **85**, 1552 (2000).
[12] Ayoub Nassour, Computational Materials Science **77**, 403 (2013).
[13] M J S P Brail, R E Nahory, F S Turco-Sandroff, H L Gilchrist, R J Martin, Appl Phys Lett **58,** 2509 (1991).
[14] Yan-Cheng Lin and Wu-Ching Chou, Nanotechnology **26,** 305704 (2015).
[15] Y. Sasaki, N. Takojima, Y. Chikarayumi, N. Kimura, T. Sawada, K. Suzuki, K. Imai, Phys.Stat. Sol. (c) **1,** 827 (2004).
[16] V.D. Ryzhikova, N.G. Starzhinskiya, L.P. Gal'chinetskiia, V. I. Silina, G. Tamulaitisb, E.K. Lisetskay, International Journal of Inorganic Materials **3**, 1227 (2001).
[17] M.M. El-Nahass, B.A. Khalifa, A.M. Abd El-Rahman, R. El-Ariny, Appl. Phys. A **63,** 81 (1996).
[18] F. Debbagh, E.L. Ameziane, M. Azizan, Sol. Energy Mater. Sol. Cells **90,** 1429 (2006).
[19] Zaoli Zhang, Thomas Wagner. Thin Solid Films **517,** 4329 (2009).
[20] Chandan Ashis Gupta, Sutanu Mangal, Udai P. Singh, Applied Surface Science **288,** 411 (2014).
[21] M. Fukuto, M.D. Hornbostel, D.C. Johnson, J. Am. Chem. Soc. **116,** 9136 (1994).
[22] R Swanepoel, J Phys E **16**, 1214 (1983).
[23] S W Wemple, M DiDomenico, J Phys Rev B **3**, 1338 (1971).